Complete eigenmode analysis of a ladder-type multiple-gap resonant cavity*

Zhang Chang-Qing(张长青)†, Ruan Cun-Jun(阮存军), Zhao Ding(赵 鼎), Wang Shu-Zhong(王树忠), and Yang Xiu-Dong(杨修东)

Key Laboratory of High Power Microwave Sources and Technologies, Institute of Electronics, Chinese Academy of Sciences, Beijing 100190, *China*

(Received 29 October 2013; revised manuscript received 6 March 2014; published online 10 June 2014)

A theoretical model is developed for calculating the eigenmodes of the multi-gap resonant cavity. The structure of concern is a kind of ladder-type circuit, offering the advantages of easy fabrication, high characteristic impedance (R/Q), and thermal capacity in the millimeter wave to THz regime. The eigenfunction expansion method is used to establish the field expressions for the gaps and the coupling region. Then, the match conditions at the interface are employed, which leads to a group of complicate boundary equations in the form of an infinite series. To facilitate the mathematical treatments and perform a highly efficient calculation, these boundary equations are transformed into the algebraic forms through the matrix representations. Finally, the concise dispersion equation is obtained. The roots of the dispersion equation include both the axial modes in the gaps, which include the fundamental and the high-order modes, and the cavity modes in the coupling region. Extensive numerical results are presented and the behaviors of the multi-gap resonant cavity are examined.

Keywords: multi-gap resonant cavity, ladder-type circuit, eigenfunction expansion, mode spectrum

PACS: 84.40.Dc, 03.50.De, 41.20.–q, 84.40.Fe **DOI:** 10.1088/1674-1056/23/8/088401

1. Introduction

Multi-gap resonant cavities (MRCs), each of which consists of more than one discrete interaction gap coupled through the slot or tunnel, are widely used in vacuum electrics such as klystrons,[1–4] extended interaction klystrons (EIK),[5–9] and extended interaction oscillators (EIO).[10–13] The MRC is characterized by the improved performances in characteristic impedance (R/Q), power capacity, and interaction efficiency. With the resonant and periodic characteristics combined, the MRC is practically regarded as a mixture of the resonant cavity and the slow-wave structure (SWS). In particular, the MRC is readily derived from the SWS,[14–19] such as the Hughes-type coupled cavity circuit which can be taken as a typical example.[20] Thus, in principle, there are possibly two ways to analyze a multi-gap resonant cavity, namely, the resonant cavity theory or the SWS. However, only the double-gap and the triple-gap cavity have been extensively studied up to now,[21–23] and most of these studies are based on the equivalent circuit model. It is not straightforward to extend these analyses to the more general cases with arbitrary gaps because the modes would become much more complicated as the number of gaps increases. On the other hand, although the dispersion relation and the synchronism can be revealed based on the SWS theory, the complete mode spectrum cannot be identified for the MRC.

In this paper the characteristics of the MRC, especially the mode distribution, will be investigated based on the general theory of the resonant cavity. The structure under study is a kind of ladder-type circuit as shown in Fig. 1, which is characterized by the planar geometry compatible with the micro-electro-mechanical system (MEMS) fabrication technology. Such is a satisfying interaction circuit that offers advantages in easy fabrication, high characteristic impedance (R/Q), and thermal capacity, which is promising for millimeter wave and THz device applications.[24,25] Although the circuit seems to be simple in geometry, it supports a number of modes which are quite complicated in distribution. Thus, great efforts have been made to establish the dispersion relation by using the eigenfunction expansion method, which can provide a thorough mode analysis.

2. Theory

Cartesian coordinates (x, y, z) are employed to describe the geometry of the ladder-type MRC in Fig. 1. The structure has a uniform depth w in the x direction. The width of the gap is denoted by d; the periodic spacing between two adjacent gaps is denoted by p; the half height of the gaps is h; the distance from the central plane of the gap to the top surface of the upper coupled cavity is H_t; the distance to the bottom surface of the lower coupled cavity is H_b. Obviously, the case, $H_t = H_b$, corresponds to a symmetric structure.

*Project supported by the National Natural Science Foundation of China (Grant Nos. 61222110 and 60971073).

†Corresponding author. E-mail: c.q.zhang@163.com

© 2014 Chinese Physical Society and IOP Publishing Ltd

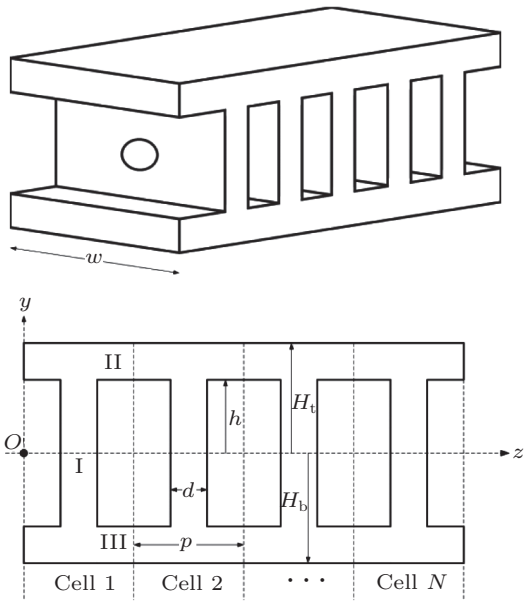


Fig. 1. Schematic illustration of the ladder-type multi-gap resonant cavity.

2.1. Representations of the electromagnetic fields

Since the structure itself is invariant in the x direction, the normal modes in such a structure can be classified as the transverse electric (TE) and transverse magnetic (TM) mode with respect to the x direction. The modes of interest are the TE$^{(x)}$ ones, each of which has a dominant electric component in the z direction. For the TE$^{(x)}$ modes, $E_x = 0$ and H_x satisfy the scalar wave equation

$$\nabla^2 H_x(x,y,z) + k_0^2 H_x(x,y,z) = 0, \tag{1}$$

where $k_0^2 = \omega^2 \mu_0 \varepsilon_0$.

The solution of Eq. (1) can be written as $H_x(x,y,z) = X(x)Y(y)Z(z)$, where X, Y, and Z are the harmonic functions in the Cartesian coordinate system. For the closed cavity the harmonic functions are $\{\sin(ku), \cos(ku)\}$ or $\{\sinh(ku), \cosh(ku)\}$, corresponding to the standing wave or the evanescent wave respectively. Considering the conductor boundary condition in the x direction, a similar behavior of H_x with respect to x in all three directions can be determined, i.e., $X(x) \sim \sin(k_x x)$, where $k_x = l\pi/w$, $l = 1, 2, 3 \ldots$. Applying the other conductor boundary condition in each region, i.e., $\boldsymbol{n} \cdot \nabla H_x = 0$, where $\boldsymbol{n}$ is normal to the boundary, we can obtain the following expressions:

inside the gaps (region 1: $-h \le y \le h$)

$$H_{x,\mathrm{I}}^{(i)} = \sum_{s=0}^{\infty} \sin(k_x x) \left[A_s^{(i)} F_s(y) + B_s^{(i)} K_s(y) \right] \times \cos\left[k_{zs,\mathrm{I}} \left(z - z_0^{(i)} \right) \right], \tag{2}$$

where

$$F_s(y) = \begin{cases} \sin(k_{ys,\mathrm{I}} y), & k_{ys,\mathrm{I}}^2 > 0, \\ \sinh(t_{ys,\mathrm{I}} y), & k_{ys,\mathrm{I}}^2 < 0, \end{cases} \tag{3}$$

$$K_s(y) = \begin{cases} \cos(k_{ys,\mathrm{I}} y), & k_{ys,\mathrm{I}}^2 > 0, \\ \cosh(t_{ys,\mathrm{I}} y), & k_{ys,\mathrm{I}}^2 < 0, \end{cases} \tag{4}$$

and

$$k_{zs,\mathrm{I}} = \frac{s\pi}{d}, \quad s = 0, 1, 2, \ldots,$$
$$k_{ys,\mathrm{I}}^2 = k_0^2 - k_x^2 - k_{zs,\mathrm{I}}^2 = k_\mathrm{c}^2 - k_{zs,\mathrm{I}}^2 = -t_{ys,\mathrm{I}}^2,$$
$$z_{0,i} = \sum_{k=0}^{i-1} p_k, \quad i = 1, 2, \ldots, N.$$

In region 2 ($h \le y \le H_\mathrm{t}$)

$$H_{x,\mathrm{II}} = \sum_{q=0}^{\infty} C_q \sin(k_x x) G_q(y) \cos\left(k_{zq,\mathrm{II}} z\right), \tag{5}$$

where

$$G_q(y) = \begin{cases} \cos\left[k_{yq,\mathrm{II}} (H_t - y)\right], & k_{yq,\mathrm{II}}^2 > 0, \\ \cosh\left[t_{yq,\mathrm{II}} (H_t - y)\right], & k_{yq,\mathrm{II}}^2 < 0, \end{cases} \tag{6}$$

and

$$k_{zq,\mathrm{II}} = \frac{q\pi}{L}, \quad L = Np, \quad q = 0, 1, 2, \ldots,$$
$$k_{yq,\mathrm{II}}^2 = k_0^2 - k_x^2 - k_{zq,\mathrm{II}}^2 = k_\mathrm{c}^2 - k_{zq,\mathrm{II}}^2 = -t_{yq,\mathrm{II}}^2.$$

In region 3 ($-H_\mathrm{b} \le y \le -h$)

$$H_{x,\mathrm{III}} = \sum_{m=0}^{\infty} D_m \sin(k_x x) P_m(y) \cos\left(k_{zq,\mathrm{III}} z\right), \tag{7}$$

where

$$P_m(y) = \begin{cases} \cos\left[k_{ym,\mathrm{III}} (H_b + y)\right], & k_{ym,\mathrm{III}}^2 > 0, \\ \cosh\left[t_{ym,\mathrm{III}} (H_b + y)\right], & k_{ym,\mathrm{III}}^2 < 0, \end{cases} \tag{8}$$

and

$$k_{zm,\mathrm{III}} = \frac{m\pi}{L}, \quad L = Np, \quad m = 0, 1, 2, \ldots,$$
$$k_{yq,\mathrm{III}}^2 = k_0^2 - k_x^2 - k_{zm,\mathrm{III}}^2 = k_\mathrm{c}^2 - k_{zm,\mathrm{III}}^2 = -t_{ym,\mathrm{III}}^2.$$

The superscript i in the field expressions of region 1 denotes the i-th gap. Obviously, the field expressions have the same form for identical gaps. However, the amplitudes of the fields may vary with the gap position for different axial modes due to the coupling between gaps, which is characterized by the coefficients $A_s^{(i)}$ and $B_s^{(i)}$.

The expressions of the transverse field components can be readily derived from H_x using Maxwell equations:

$$\begin{cases} E_y = -\dfrac{\mathrm{j}\omega\mu_0}{k_\mathrm{c}^2} \dfrac{\partial H_x}{\partial z}, \\ E_z = \dfrac{\mathrm{j}\omega\mu_0}{k_\mathrm{c}^2} \dfrac{\partial H_x}{\partial y}, \end{cases} \quad \begin{cases} H_y = \dfrac{1}{k_\mathrm{c}^2} \dfrac{\partial^2 H_x}{\partial y \partial x}, \\ H_z = \dfrac{1}{k_\mathrm{c}^2} \dfrac{\partial^2 H_x}{\partial z \partial x}, \end{cases} \tag{9}$$

where $k_\mathrm{c}^2 = k_0^2 - k_x^2$. Here, we just give the concrete form of the E_z component, because it will be used in the boundary matching procedure. Thus, by substituting Eqs. (2), (5), and (7) into Eq. (9), we obtain the following results.

In region 1:

$$E_{z,\mathrm{I}}^{(i)} = \frac{\mathrm{j}\omega\mu_0}{k_{\mathrm{c}}^2}\sum_{s=0}^{\infty}\sin(k_x x)\left[A_s^{(i)}F_s'(y)+B_s^{(i)}K_s'(y)\right] \times\cos\left[k_{zs,\mathrm{I}}\left(z-z_0^{(i)}\right)\right], \tag{10}$$

where

$$F_s'(y)=\begin{cases} k_{ys,\mathrm{I}}\cos(k_{ys,\mathrm{I}}y), & k_{ys,\mathrm{I}}^2>0,\\ t_{ys,\mathrm{I}}\cosh(t_{ys,\mathrm{I}}y), & k_{ys,\mathrm{I}}^2<0,\end{cases} \tag{11a}$$

$$K_s'(y)=\begin{cases} -k_{ys,\mathrm{I}}\sin(k_{ys,\mathrm{I}}y), & k_{ys,\mathrm{I}}^2>0,\\ t_{ys,\mathrm{I}}\sinh(t_{ys,\mathrm{I}}y), & k_{ys,\mathrm{I}}^2<0.\end{cases} \tag{11b}$$

In region 2:

$$E_{z,\mathrm{II}} = \frac{\mathrm{j}\omega\mu_0}{k_{\mathrm{c}}^2}\sum_{q=0}^{\infty}C_q\sin(k_x x)G_q'(y)\cos\left(k_{zq,\mathrm{II}}z\right), \tag{12}$$

where

$$G_q'(y)=\begin{cases} k_{yq,\mathrm{II}}\sin\left[k_{yq,\mathrm{II}}(H_t-y)\right], & k_{yq,\mathrm{II}}^2>0,\\ -t_{yq,\mathrm{II}}\sinh\left[t_{yq,\mathrm{II}}(H_t-y)\right], & k_{yq,\mathrm{II}}^2<0.\end{cases} \tag{13}$$

In region 3:

$$E_{z,\mathrm{III}} = \frac{\mathrm{j}\omega\mu_0}{k_{\mathrm{c}}^2}\sum_{m=0}^{\infty}D_m\sin(k_x x)P_m'(y)\cos(k_{zm,\mathrm{III}}z), \tag{14}$$

where

$$P_m'(y)=-k_{ym,\mathrm{III}}\sin\left[k_{ym,\mathrm{III}}(H_b+y)\right],\quad k_{ym,\mathrm{III}}^2>0,$$
$$t_{ym,\mathrm{III}}\sinh\left[t_{ym,\mathrm{III}}(H_b+y)\right],\quad k_{ym,\mathrm{III}}^2<0. \tag{15}$$

2.2. Application of the boundary conditions

At the interface $y=h$

$$H_{x,\mathrm{II}}=H_{x,\mathrm{I}}^{(i)},\quad z_0^{(i)}\le z\le z_0^{(i)}+d, \tag{16a}$$

$$E_{z,\mathrm{II}}=\begin{cases} E_{z,\mathrm{I}}^{(i)}, & z_0^{(i)}\le z\le z_0^{(i)}+d,\\ 0, & z_0^{(i)}+d\le z\le z_0^{(i)}+p.\end{cases} \tag{16b}$$

At the interface $y=-h$,

$$H_{x,\mathrm{III}}=H_{x,\mathrm{I}}^{(i)},\ z_0^{(i)}\le z\le z_0^{(i)}+d, \tag{17a}$$

$$E_{z,\mathrm{III}}=\begin{cases} E_{z,\mathrm{I}}^{(i)}, & z_0^{(i)}\le z\le z_0^{(i)}+d,\\ 0, & z_0^{(i)}+d\le z\le z_0^{(i)}+p.\end{cases} \tag{17b}$$

Substituting Eqs. (2) and (5) into the boundary condition (16a) yields

$$\sum_{q=0}^{\infty}C_qG_q(h)\cos\left(k_{zq,\mathrm{II}}z\right) = \sum_{s=0}^{\infty}\left[A_s^{(i)}F_s(h)+B_s^{(i)}K_s(h)\right]\cos\left[k_{zs,\mathrm{I}}\left(z-z_0^{(i)}\right)\right]. \tag{18}$$

By multiplying both sides of Eq. (18) by $\cos[k_{zs',\mathrm{I}}(z-z_0^{(i)})]$ and integrating the product over z from $z=z_0^{(i)}$ to $z=z_0^{(i)}+d$, with the orthogonality considered, then we will obtain

$$A_s^{(i)}F_s(h)(1+\delta_{s,0})+B_s^{(i)}K_s(h)(1+\delta_{s,0}) = \frac{2}{d}\sum_{q=0}^{\infty}C_qG_q(h)\Theta\left(k_{zs,\mathrm{I}},k_{zq,\mathrm{II}},i\right), \tag{19}$$

where

$$\Theta\left(k_{zs,\mathrm{I}},k_{zq,\mathrm{II}},i\right) = \int_{z_0^{(i)}}^{z_0^{(i)}+d}\cos\left[k_{zs,\mathrm{I}}\left(z-z_0^{(i)}\right)\right]\times\cos\left(k_{zq,\mathrm{II}}z\right)\mathrm{d}z. \tag{20}$$

Equation (20) is the partial integral associated with the gap index i. This integral can be solved analytically, the result is

$$\Theta\left(k_{zs,\mathrm{I}},k_{zq,\mathrm{II}},i\right)=\begin{cases} d,\ k_{zs,\mathrm{I}}=k_{zq,\mathrm{II}}=0,\\ \dfrac{d}{2}\cos\left(k_{zs,\mathrm{I}}z_0^{(i)}\right),\ k_{zs,\mathrm{I}}=k_{zq,\mathrm{II}}\neq 0,\\ \dfrac{k_{zq,\mathrm{II}}\left\{(-1)^{-s}\sin\left[k_{zq,\mathrm{II}}\left(z_0^{(i)}+d\right)\right]-\sin\left(k_{zq,\mathrm{II}}z_0^{(i)}\right)\right\}}{k_{zq,\mathrm{II}}^2-k_{zs,\mathrm{I}}^2},\quad k_{zs,\mathrm{I}}\neq k_{zq,\mathrm{II}}.\end{cases}$$

Similarly, from Eqs. (2), (7), and (17a), we have

$$A_s^{(i)}F_s(-h)(1+\delta_{s,0})+B_s^{(i)}K_s(-h)(1+\delta_{s,0}) = \frac{2}{d}\sum_{m=0}^{\infty}D_mP_m(-h)\Theta\left(k_{zs,\mathrm{I}},k_{zm,\mathrm{II}},i\right). \tag{21}$$

Next, we turn to the continuity conditions of the electric field, namely, Eqs. (16b) and (17b). In order to express C_q and D_m as the superposition of $A_s^{(i)}$ and $B_s^{(i)}$, we need to multiply both sides of the equations by $\cos(k_{zq,\mathrm{II}}z)$ and integrate over z from 0 to L. This means that the integral in the right of the equations will cover all the gaps. Since the gaps are discrete, equations (16b) and (17b) become

$$\int_0^L E_{z,\mathrm{II}} \cos\left(k_{zq',\mathrm{II}} z\right) \mathrm{d}z = \sum_{i=1}^{N} \left[\int_{z_0^{(i)}}^{z_0^{(i)}+d} E_{z,\mathrm{II}}^{(i)} \cos\left(k_{zq',\mathrm{II}} z\right) \mathrm{d}z \right], \tag{22}$$

$$\int_0^L E_{z,\mathrm{III}} \cos\left(k_{zm',\mathrm{III}} z\right) \mathrm{d}z = \sum_{i=1}^{N} \left[\int_{z_0^{(i)}}^{z_0^{(i)}+d} E_{z,\mathrm{I}}^{(i)} \cos\left(k_{zm',\mathrm{III}} z\right) \mathrm{d}z \right]. \tag{23}$$

By substituting Eqs. (10), (12), and (14) into Eqs. (22) and (23), the following equations are obtained

$$C_q G_q'(h)\left(1+\delta_{q,0}\right) = \frac{2}{L} \sum_{i=1}^{N} \sum_{s=0}^{\infty} \left[A_s^{(i)} F_s'(h) + B_s^{(i)} K_s'(h) \right] \times \Theta\left(k_{zq,\mathrm{II}}, k_{zs,\mathrm{I}}, i\right), \tag{24}$$

$$D_m P_m'(-h)\left(1+\delta_{m,0}\right) = \frac{2}{L} \sum_{i=1}^{N} \sum_{s=0}^{\infty} \left[A_s^{(i)} F_s'(-h) + B_s^{(i)} K_s'(-h) \right] \times \Theta\left(k_{zm,\mathrm{III}}, k_{zs,\mathrm{I}}, i\right). \tag{25}$$

According to Eqs. (3) and (4) which are the definitions of $F_s(y)$ and $K_s(y)$, we have $F_s(-h) = -F_s(h)$, $K_s(-h) = K_s(h)$. Thus, equations (19) and (21) can be rewritten as

$$A_s^{(i)} F_s(h)\left(1+\delta_{s,0}\right) = \frac{1}{d} \sum_{q=0}^{\infty} C_q G_q(h) \Theta\left(k_{zs,\mathrm{I}}, k_{zq,\mathrm{II}}, i\right) - \frac{1}{d} \sum_{m=0}^{\infty} D_m P_m(-h) \Theta\left(k_{zs,\mathrm{I}}, k_{zm,\mathrm{II}}, i\right), \tag{26}$$

$$B_s^{(i)} K_s(h)\left(1+\delta_{s,0}\right) = \frac{1}{d} \sum_{q=0}^{\infty} C_q G_q(h) \Theta\left(k_{zs,\mathrm{I}}, k_{zq,\mathrm{II}}, i\right) + \frac{1}{d} \sum_{m=0}^{\infty} D_m P_m(-h) \Theta\left(k_{zs,\mathrm{I}}, k_{zm,\mathrm{II}}, i\right). \tag{27}$$

2.3. Matrix dispersion equation

We have obtained a complete set of equations, Eqs. (24)–(27), which determine the eigenvalue problem of the planar ladder-type MRC. However, it can be quite involved and inefficient to directly solve these equations due to the coupled integral–summation operation. Thus, equations (24)–(27) are transformed into the matrix equivalents, which are

$$\Delta_s F(h) A^{(i)} = \frac{1}{d} \bar{\Theta}_{SQ} G(h) C - \frac{1}{d} \bar{\Theta}_{SM} P(-h) D, \tag{28a}$$

$$\Delta_s K(h) B^{(i)} = \frac{1}{d} \bar{\Theta}_{SQ} G(h) C + \frac{1}{d} \bar{\Theta}_{SM} P(-h) D, \tag{28b}$$

$$\Delta_Q G'(h) C = \frac{2}{L} \sum_{i=1}^{N} \left[\bar{\Theta}_{QS}^{(i)} F'(h) A^{(i)} + \Theta_{QS}^{(i)} K'(h) B^{(i)} \right], \tag{28c}$$

$$\Delta_M P'(-h) D = \frac{2}{L} \sum_{i=1}^{N} \left[\bar{\Theta}_{MS}^{(i)} F'(-h) A^{(i)} + \Theta_{mS}^{(i)} K'(-h) B^{(i)} \right], \tag{28d}$$

where $A^{(i)}$, $B^{(i)}$, C, and D are the column vectors which have the general form of

$$A^{(i)} = \left[A_0^{(i)} \; A_1^{(i)} \; A_2^{(i)} \; \cdots \; A_{N_s}^{(i)} \; \right]^{\mathrm{T}}. \tag{29}$$

The dimensions of $A^{(i)}$, $B^{(i)}$, C, and D are N_s+1, N_s+1, N_q+1, and N_m+1 respectively, where N_s, N_q, N_m are the numbers from which the infinite summations are truncated. $F(h)$, $K(h)$, $G(h)$, and $P(h)$ are all the diagonal matrices that have the same form, which is

$$F(h) = \mathrm{diag}\left[F_0(h) \; F_1(h) \; F_2(h) \; \cdots \; F_{N_s}(h) \; \right]. \tag{30}$$

The symbol $\triangle$ denotes a diagonal matrix evolved from the δ-function and it has the form of

$$\Delta_S = \mathrm{Diag}\left[\underbrace{2 \; 1 \; 1 \; \cdots \; 1}_{S+1} \right]. \tag{31}$$

It should be pointed out that the dimension of the matrix is indicated by the subscript. For example, $\bar{\Theta}_{SQ}$ is a matrix with a dimension of $(N_s+1)\times(N_q+1)$. With the dimension properly defined, equations (28a)–(28d) are self-consistent for arbitrary numbers of N_s, N_q, and N_m.

Substituting Eqs. (28a) and (28b) into Eqs. (28c) and (28d), we finally obtain the system of equations with the following structures:

$$\frac{1}{2} L d \Delta_Q G'(h) C = \left(\Xi_1 C - \Xi_2 D\right), \tag{32a}$$

$$\frac{1}{2} L d \Delta_Q P'(-h) D = \left(\Xi_3 C - \Xi_4 D\right), \tag{32b}$$

where

$$\Xi_1 = \sum_{i=1}^{N} \bar{\Theta}_{QS}^{(i)} \{ F'(h) \left[\Delta_S F(h)\right]^{-1} + K'(h) \left[\Delta_S K(h)\right]^{-1} \} \bar{\Theta}_{SQ}^{(i)} G(h), \tag{33a}$$

$$\Xi_2 = \sum_{i=1}^{N} \bar{\Theta}_{QS}^{(i)} \{ F'(h) \left[\Delta_S F(h)\right]^{-1} - K'(h) \left[\Delta_S K(h)\right]^{-1} \} \bar{\Theta}_{SM}^{(i)} P(-h), \tag{33b}$$

$$\Xi_3 = \sum_{i=1}^{N} \bar{\Theta}_{MS}^{(i)} \{ F'(-h) \left[\Delta_S F(h)\right]^{-1} + K'(-h) \left[\Delta_S K(h)\right]^{-1} \} \bar{\Theta}_{SQ}^{(i)} G(h), \tag{33c}$$

$$\Xi_4 = \sum_{i=1}^{N} \bar{\Theta}_{MS}^{(i)} \{ F'(-h) \left[\Delta_S F(h)\right]^{-1} - K'(-h) \left[\Delta_S K(h)\right]^{-1} \} \bar{\Theta}_{SM}^{(i)} P(-h). \tag{33d}$$

The eigenvalue problem of Eqs. (32a) and (32b) concludes the analytic formulae. The dispersion equation is obtained by setting the determinant to be zero, i.e.,

$$\begin{pmatrix} \Xi_1 - \frac{1}{2} L d \Delta_Q G'(h) & -\Xi_2 \\ \Xi_3 & -\frac{1}{2} L d \Delta_Q P'(-h) - \Xi_4 \end{pmatrix} = 0. \tag{34}$$

In such a system, the roots of Eq. (34) correspond to the eigenfrequencies of the $\mathrm{TE}^{(x)}$ modes supported by the structure. The distribution of the modes depends on the sequence of the roots. It is helpful to define the denotations for these modes. Like the conventional resonant cavity, we use the modes in the gaps to define the transverse index. For example, the notation of $\mathrm{TE}_{10}^{(x)}$ denotes the fundamental mode in the gaps, where the index 1 and 0 correspond to the y and z directions respectively. The absence of the x-directional index is due to its uniformity in all the three regions, which is a precondition in the calculation. However, for the multi-gap cavity the axial index also needs to be specified, thus the combined notation is used, i.e. $\mathrm{TE}_{10}^{(x)} * [n/(N-1)]\pi$, where N is the total number of the gaps, and $n = 0, 1, 2, \ldots, N-1$.

It should be noticed that the aforementioned formulation is made for the general case of the unsymmetrical structure. If the structure is symmetric, i.e., $H_\mathrm{t} = H_\mathrm{b}$, the system becomes simpler. By applying the magnetic and the electric walls to the xz-plane, the eigenvalue problem can be divided into two independent cases. In each case, the three regions will be reduced into two regions, because only one set of coefficients $A_s^{(i)}$ or $B_s^{(i)}$ is required. The dispersion equations for the symmetric structure are given in the Appendix A.

3. Numerical results and discussion

The convergence of the numerical calculations must be examined before further performing the analysis. This is done by using a double-gap cavity. It is known that a double-gap cavity supports two axial modes, i.e., 2π mode (the electric fields are in the same direction in the two gaps) and π mode (the electric fields are in the opposite directions in the two gaps). The geometrical parameters of the double-gap cavity are as follows: $w = 1.8$, $d = 0.25$, $p = 0.77$, $h = 0.6$, $H_\mathrm{t} = H_\mathrm{b} = 1.0$, the unit is millimeter (mm). In the calculation, we set $l = 1$, which means that only the fundamental mode in the x direction is considered. Figure 2 shows the convergences of the 2π mode and π mode with respect to N_s and N_q, where the general dispersion equation (34) is used. From Fig. 2 it can be seen that good convergences have been achieved for both modes when $N_s > 10$ and $N_q > 25$. Thus, $N_s = 15$ and $N_q = 35$ will be used in the subsequent calculations to compromise accuracy and efficiency.

Because the structure is symmetric in this example, the simplified dispersion equation (A8) can also be used. The results are listed in Table 1. The numerical results of the theory are compared with the three-dimensional (3D) electromagnetic simulation results by using CST-MWS. It can be seen that they accord with each other very well.

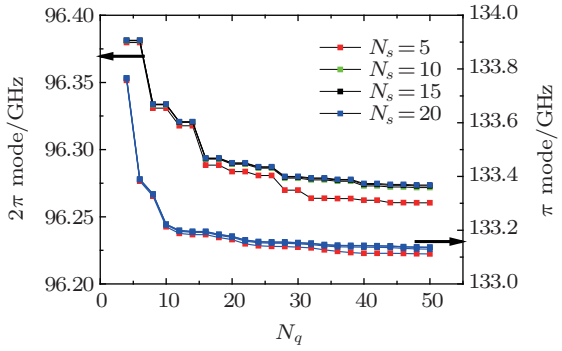


Fig. 2. (color online) Convergences of the numerical calculations.

Table 1. Comparisons of the results between the theory and simulation for a double-gap cavity.

Mode sequence	Theory		CST-MWS
	Magnetic wall	Electrical wall	
1	96.2784	110.3389	96.2435
2	133.1429	151.094	110.263
3		162.9812	133.090
4			150.836
5			162.774

The simplified dispersion equation (A8) under the magnetic wall condition (A2) is found to have two roots that correspond to the 2π mode and π mode. With the notation defined, the two modes can be denoted by $\mathrm{TE}_{10}^{(x)} * 2\pi$ and $\mathrm{TE}_{10}^{(x)} * \pi$. The magnetic wall modes are symmetric modes whose axial electric field is symmetric with respect to the y axis as shown in Fig. 3(a). Thus, these modes can effectively interact with an electron beam.

The equation (A8) under the electrical wall condition (A3) is found to have three roots. The first one is a cavity mode which exists in the coupled regions; the others are the modes in the gaps which are antisymmetric modes with respect to the y axis, as shown in Fig. 3(b). Actually, the antisymmetric modes are the first higher-order gap modes in the y direction, which can be denoted by $\mathrm{TE}_{20}^{(x)} * 2\pi$ and $\mathrm{TE}_{20}^{(x)} * \pi$. It can be seen that the higher-order gap modes also have axial variations. Therefore, each kind of transverse mode in the gap can form a mode band due to the axial distribution. From Table 1, we can find that the two bands of axial modes of the $\mathrm{TE}_{10}^{(x)}$-cluster and $\mathrm{TE}_{20}^{(x)}$-cluster do not overlap, with the frequency of the $\mathrm{TE}_{20}^{(x)} * 2\pi$ mode being higher than that of the $\mathrm{TE}_{10}^{(x)} * \pi$ mode. However, things are different from the resonant cavity with more gaps.

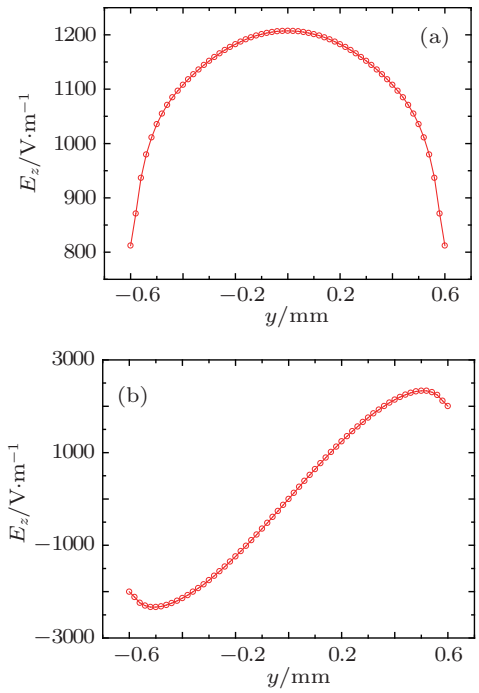


Fig. 3. (color online) Electric field profiles of the E_z component in the y direction at $x = w/2$ and $z = z_0^{(1)}$.

The mode spectra of the three-gap, four-gap, and five-gap cavities are separately shown in Figs. 4–6, where the first two axial mode bands are considered. It can be seen that both bands are enlarged as the number of gaps increases due to the increase in the frequency of the π mode. The second band is much narrower than the first one, and hence the separation of the modes is much smaller. Unlike the double-gap cavity, the two axial mode bands overlap with each other for the cavity with more gaps. As the gap number increases, more axial modes of the second band will fall into the first band, which are densely distributed around the $\mathrm{TE}_{10}^{(x)} * \pi$ mode.

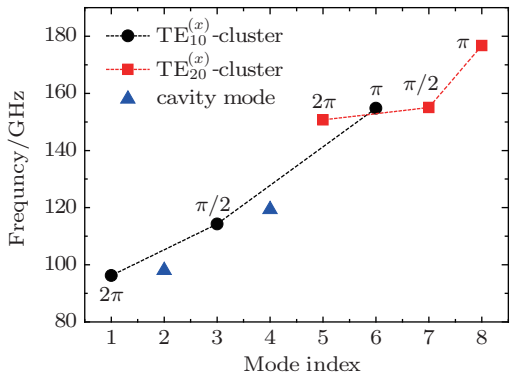


Fig. 4. (color online) Mode spectra of the three-gap cavity.

The number of the axial modes of each band is equal to the number of gaps. In other words, the N-gap cavity supports N axial modes for one kind of gap mode. As we have mentioned, the axial modes are characterized by the different numbers of axial variations. This characteristic is clearly illustrated in Fig. 7, taking the five-gap cavity as an example. These figures show the variations of the on-axial electric field E_z in magnitude and direction with the index of gaps for $\mathrm{TE}_{10}^{(x)}$-cluster modes. Obviously, the 2π mode results in invariant on-axial electric field both in magnitude and direction. For the $\pi/4$ mode and $3\pi/4$ mode, the on-axial electric field vanishes in the third gap, so, it is absent in the figure.

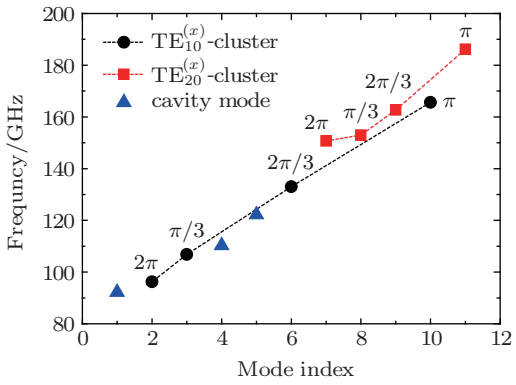


Fig. 5. (color online) Mode spectrum of the four-gap cavity.

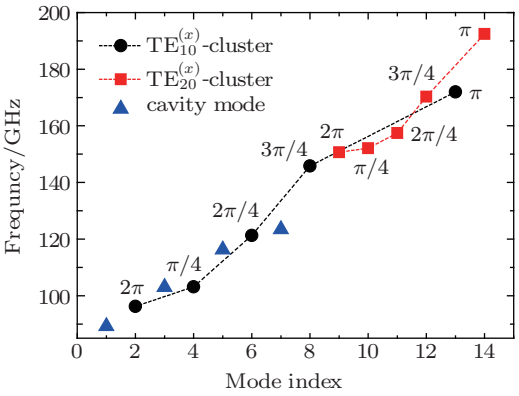


Fig. 6. (color online) Mode spectrum of the five-gap cavity.

The mode spectra reveal that stable operation can be achieved under the $\mathrm{TE}_{10}^{(x)} * 2\pi$ mode. Firstly, large mode separation can be obtained between the $\mathrm{TE}_{10}^{(x)} * 2\pi$ mode and the adjacent axial modes, such as the $\mathrm{TE}_{10}^{(x)} * \pi/4$ mode of the five-gap cavity. Moreover, there are no higher-order gap modes in the vicinity of the $\mathrm{TE}_{10}^{(x)} * 2\pi$ mode, but some cavity modes. The axial electric fields of the cavity modes are much weaker than those of the gap modes. Thus, the cavity modes cannot harm the stability if there is a sufficient separation from the operating mode.

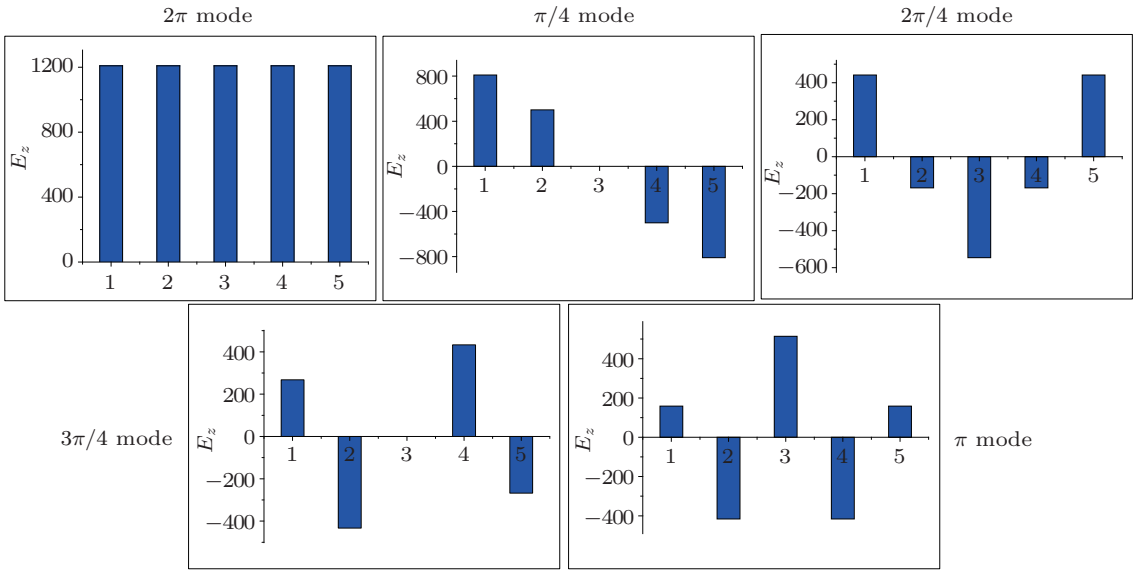


Fig. 7. (color online) E_z electric fields along the z axis for different axial modes.

Figure 8 shows the variations of the mode separation of the first five modes of the five-gap cavity with geometry parameter H_b. This analysis corresponds to the tuning effect in practice. It can be seen that the $TE_{10}^{(x)} * 2\pi$ mode is sensitive to H_b. The frequency of the $TE_{10}^{(x)} * 2\pi$ mode varies over 1 GHz as H_b is varied within 0.1 mm. At the same time the $TE_{10}^{(x)} * 2\pi$ mode keeps a sufficiently large separation from the adjacent cavity modes. At the high-frequency end, where $H_b = 0.36$ mm, the separation between the $TE_{10}^{(x)} * 2\pi$ mode and the second cavity mode is 5.89 GHz; at the low-frequency end, where $H_b = 0.45$ mm, the separation between the $TE_{10}^{(x)} * 2\pi$ mode and first cavity mode is 6.28 GHz. With such a large separation between modes, we can safely use the five-gap cavity to achieve higher gain and bandwidth in the design.

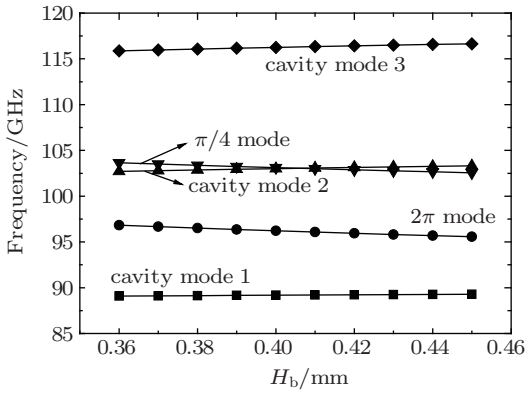


Fig. 8. Variations of mode separation of the five-gap cavity with H_b.

Figure 9 reveals the periodic property of the MRC in comparison with that of the ideal SWS. It can be seen that the equivalent dispersion curves of the MRC approach those of the ideal SWS as the number of gaps increases. The approaching process is characterized by the gradually lifted end of π mode and the stable end of 2π mode. However, when the cavity consists of only several gaps, i.e., three or five gaps, the curves are quite different from that of the ideal periodic circuit. The nonlinear variation around the π-mode end in the dispersion curve can be observed only when the number of gaps is sufficiently large. As shown in the figure, for the case of 30 gaps, the equivalent dispersion curve of the multi-gap cavity is nearly identical to that of the ideal periodic circuit. Moreover, although we name the modes by equal phase shift, the frequencies of the axial modes are not equally distributed. Near the end of the 2π mode, the frequency separations of the modes are much less than those in the case of the mid-part curve.

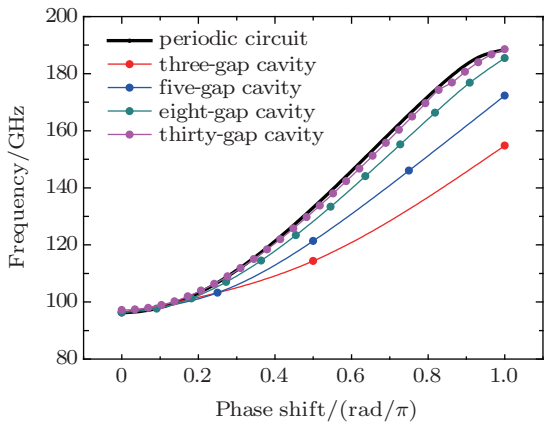


Fig. 9. (color online) Variations of equivalent dispersion characteristics of the multi-gap cavity with the number of gaps, compared with the dispersion curve of the ideal periodic circuit.

It is noted that the frequency of the 2π mode is stable and identical to the frequency of the 2π-end of the ideal SWS. The reason why the frequency of the 2π mode is independent of the number of gaps is that the 2π mode corresponds to the case where each cell is resonant itself. When all the structure cells are identical, they have the same resonant frequency that is just the frequency of the 2π mode. Such a property is useful, because we can use only one cell to represent the whole cavity when it is designed to operate at 2π mode. This could help to facilitate the design and significantly lessen the burden of calculations.

4. Conclusion

The planar ladder-type multi-gap resonant cavity which is simple in geometry but complicated in mode distribution is investigated. The developed theoretical model is proven to be valid and highly efficient in the analysis of the modes of this kind of interaction circuit. The eigenfunction expansion method is used to establish the dispersion relation for the modes, which include (i) the axial mode with symmetrical field profile; (ii) the axial mode with asymmetrical field profile; and (iii) the modes in the coupled region (cavity mode). Thus, the developed model provides a useful tool for the cavity design, especially when optimizing the mode separation to ensure the stability.

Appendix A

For a symmetry structure, i.e., $H_{\rm t} = H_{\rm b}$, the wave function H_x for the TE$^{(x)}$ mode in region 1 can be written as

$$H_{x,\rm I}^{(i)} = \sum_{s=0}^{\infty} A_s^{(i)} \sin\left(k_x x\right) F_s\left(y\right) \cos\left[k_{zs,\rm I}\left(z - z_0^{(i)}\right)\right], \tag{A1}$$

where

$$F_s\left(y\right) = \begin{cases} \sin\left(k_{ys,\rm I} y\right), & k_{ys,\rm I}^2 > 0, \\ \sinh\left(t_{ys,\rm I} y\right), & k_{ys,\rm I}^2 < 0, \end{cases} \tag{A2}$$

which corresponds to the case of a magnetic wall in the symmetry plane; and

$$F_s\left(y\right) = \begin{cases} \cos\left(k_{ys,\rm I} y\right) & k_{ys,\rm I}^2 > 0, \\ \cosh\left(t_{ys,\rm I} y\right) & k_{ys,\rm I}^2 < 0, \end{cases} \tag{A3}$$

corresponds to the electric wall case.

Equations (19) and (24) are reduced to

$$\begin{aligned} & A_s^{(i)} F_s\left(h\right)\left(1+\delta_{s,0}\right) \\ &= \frac{2}{d} \sum_{q=0}^{\infty} C_q G_q\left(h\right) \Theta\left(k_{zs,\rm I}, k_{zq,\rm II}, i\right), \end{aligned} \tag{A4}$$

$$\begin{aligned} & C_q G_q'\left(h\right)\left(1+\delta_{q,0}\right) \\ &= \frac{2}{L} \sum_{i=1}^{N} \sum_{s=0}^{\infty} A_s^{(i)} F_s'\left(h\right) \Theta\left(k_{zq,\rm I}, k_{zs,\rm II}, i\right). \end{aligned} \tag{A5}$$

The matrix forms of the above two equations respectively are

$$\Delta_s F\left(h\right) A^{(i)} = \frac{2}{d} \bar{\Theta}_{SQ}^{(i)} \left[G\left(h\right) C\right], \tag{A6}$$

$$\Delta_Q G'\left(h\right) C = \frac{2}{L} \sum_{i=1}^{N} \bar{\Theta}_{QS}^{(i)} \left[F'\left(h\right) A^{(i)}\right]. \tag{A7}$$

By combining Eqs. (A6) and (A7), we can obtain the dispersion equation for the case of a magnetic wall and an electric wall, which is given by

$$\det\left(\frac{L}{2} \Delta_Q G'\left(h\right) C - M\right) = 0, \tag{A8}$$

where

$$M = \frac{2}{d} \sum_{i=1}^{N} \left[\bar{\Theta}_{QS}^{(i)} F'\left(h\right) \left[\Delta_s F\left(h\right)\right]^{-1} \bar{\Theta}_{SQ}^{(i)} G\left(h\right)\right]. \tag{A9}$$

References

[1] Huang C L, Ding Y G and Wang Y 2011 *Acta Phys. Sin.* **60** 128401 (in Chinese)

[2] Wang J X, Liu G and Luo Y 2013 *Acta Phys. Sin.* **62** 078404 (in Chinese)

[3] Preist D H and Leidigh W J 1963 *IEEE Trans. Electron Dev.* **10** 201

[4] Lee T G, Konrad G T, Okazaki Y, Masaru W and Yonezawa H 1985 *IEEE Trans. Plasma Sci.* **13** 545

[5] Cui J, Luo J R, Zhu M and Guo W 2011 *Acta Phys. Sin.* **60** 051101 (in Chinese)

[6] Cui J, Luo J R, Zhu M and Guo W 2011 *Acta Phys. Sin.* **60** 061101 (in Chinese)

[7] Preist D H and Leidigh W J1964 *IEEE Trans. Electron Dev.* **11** 369

[8] Steer B, Roitman Albert, Horoyski P, Hyttinen Mark, Dobbs R and Berry D 2007 16*th IEEE International Pulsed Power Conference*, June 17–22, Albuquerque, NM, Vol. 2, p. 1049

[9] He J, Wei Y Y, Gong Y B and Wang W X 2011 *Chin. Phys. B* **20** 054102

[10] Gao P, John H B, Yang Z H, Li B, Xu L, He J, GongY B and Tian Z 2010 *Acta Phys. Sin.* **59** 8484 (in Chinese)

[11] Zhang K C, Wu Z H and Liu S G 2008 *Chin. Phys. B* **17** 3402

[12] Zhang K C, Wu Z H and Liu S G 2009 *J. Infrared Milli Terahz Waves* **30** 309

[13] Chen L M, Guo H Z, Chen H Y, Tsao M H, Yang Tz Te, Tsai Y C and Chu K R 2000 *IEEE Trans. Plasma Sci.* **28** 626

[14] Liu Y, Xu J, Lai J Q, Xu X, Shen F, Wei Y Y, Huang M Z, Tang T and Gong Y B 2012 *Chin. Phys. B* **21** 074202

[15] Lai J Q, Wei Y Y, Xu X, Shen F, Liu Y, Liu Y, Huang M Z, Tang T and Gong Y B 2012 *Acta Phys. Sin.* **61** 178501 (in Chinese)

[16] Liu Y, Xu J, Xu X, Shen F, Wei Y Y, Huang M Z, Tang T, Wang W X and Gong Y B 2012 *Acta Phys. Sin.* **61** 154208 (in Chinese)

[17] Zhang C Q, Gong Y B, Wei Y Y and Wang W X 2010 *Acta Phys. Sin.* **59** 6653 (in Chinese)

[18] Yue L N, Wang W X, Wei Y Y and Gong Y B 2005 *Chin. Phys. Lett.* **22** 754

[19] Liu L W, Wei Y Y, Wang S M, Hou Y, Yin H R, Zhao G Q, Duan Z Y, Xu J, Gong Y B, Wang W X and Yang M H 2013 *Chin. Phys. B* **22** 108401

[20] Luo J R, Cui J, Zhu M and Guo W 2013 *Chin. Phys. B* **22** 067803

[21] Lin F M and Liu H X 2011 *Int. J. Electron.* **98** 617

[22] Shin Y M and Park G S 2004 *J. Korean Phys. Soc.* **44** 1239

[23] Ko K, Lee T G, Krollt N and Tonegawa S 1992 *Proc. SPIE* Vol. 1629, Intense Microwave and Particle Beams III, April 1

[24] Chernin D, Burke A, Chernyavskiy I, Petillo J, Dobbs R, Roitman A, Horoyski P, Hyttinen M, Berry D, Blank M, Khanh Nguyen, Jabotinsky V, Pershing D, Wright E, Calame J, Levush B, Neilson J, Gaier T, Skalare A, Barker N S, Weikle R, Booske J 2010 *IEEE International Vacuum Electronics Conference*, May 18–20, Monterey, CA, p. 217

[25] Dobbs R, Hyttinen M, Steer B, Khanh Nguyen, Wright E, Chernin D, Calame J, Levush B, Barker N S, Booske J, Blank M and Maiwald F 2011 *International Conference on Infrared, Millimeter and Terahertz Waves* (IRMMW-THz), October 2–7, Houston, TX, USA, p. 1